

# **In Situ Mapping of Normal Strains in the Field of a Growing Fatigue Crack in a Steel Weld Using Digital Image Correlation and Energy Dispersive Synchrotron X-ray Diffraction<sup>1</sup>**

T Wigger<sup>1</sup>, C Lupton<sup>1</sup>, S Alshammrei<sup>1</sup>, J Tong<sup>1\*</sup>

<sup>1</sup>Mechanical Behaviour of Materials Group, School of Engineering, University of Portsmouth, Anglesea Building, Anglesea Road, Portsmouth PO1 3DJ, UK.

T J Marrow<sup>2</sup>, P Earp<sup>2</sup>

<sup>2</sup>Department of Materials, University of Oxford, Parks Road, Oxford OX1 3PH, UK.

M-L Zhu<sup>3</sup>, D-Q Wang<sup>3</sup>

<sup>3</sup>Key Laboratory of Pressure Systems and Safety, Ministry of Education; School of Mechanical and Power Engineering, East China University of Science and Technology, Shanghai 200237, China.

T Connolley<sup>4</sup>

<sup>4</sup> I12 JEEP Beamline, Diamond Light Source synchrotron, Harwell Campus, Didcot OX11 0DE, UK.

\*Corresponding author

## **Abstract**

Fatigue crack growth in the Heat Affected Zone (HAZ) of a welded CrNiMoV steel has been investigated, *in situ*, using Digital Image Correlation (DIC) and Energy Dispersive X-Ray Diffraction (EDXD). Compact tension specimens of welded joint were loaded under tension-tension cyclic loading. The crack tip position and the evolution of the near-tip strains normal to the crack plane were tracked at selected positions for a growing fatigue crack both on the specimen surface using DIC and in the bulk of the specimen using EDXD of synchrotron X-rays. The uncertainty and quality of the DIC measurements were examined with regard to some of the key data processing parameters, including subset size and the size of measurement window; whilst the measurement errors in the

---

<sup>1</sup> This is the authors' copy of a paper accepted for publication in International Journal of Fatigue (2018)

EDXD measurements were also estimated. A “characteristic” strain was estimated, in the bulk of the specimen and on the specimen surface, from the average strains captured at selected positions when the propagating fatigue crack tip reached these positions.

## **Keywords**

Crack tip, DIC, EDXD, fatigue crack growth, HAZ, welding

## **1. Introduction**

Understanding the mechanical behaviour of defects as a result of welding is of great importance to the safety and reliability of welded engineering components and structures. Although there is a large body of work in the literature on the fatigue behaviour of welded joints, most of the studies have been empirical or semi-empirical analyses based on simple engineering principles. Previous research has shown that the nano/micro-hardness, ultimate tensile strength (UTS) and yield stress in the heat-affected zone (HAZ) differed considerably from those of base metal (BM) or weld metal (WM) [1]. The variation of mechanical properties in the HAZ was found to be related to the variation of the microstructure as a result of welding. The HAZ is known to be most susceptible to damage in the form of cracking in welded structures. Although physically short cracks in HAZ have been studied in some detail [2], steady-state fatigue crack growth behaviour in a HAZ remains an important topic to be explored for damage tolerance assessments of welds. The focus of the present study is therefore to examine the evolution of near-tip strain field in the presence of fatigue crack growth in the HAZ towards a crack growth criterion by identifying a strain “onset” or a “critical strain” at the moment of crack growth.

Fatigue crack growth in engineering applications has been characterised by the range of stress intensity factor  $\Delta K$  [3] under small scale yielding conditions. The micro-mechanical characteristics near the crack tip are not considered in such a global approach, yet crack growth can only occur if locally the material ahead the crack tip fails. We hypothesized [4] that fatigue crack growth would occur when the accumulation of maximum principal strain, or normal strain, reaches a “critical” value for material separation [5]. We have tested this hypothesis using a number of numerical simulation

tools [4,5] and found significant ratchetting of normal strain near the crack tip with fatigue cycles, independent of material or specimen geometry. We have since carried out experimental studies using the Digital Image Correlation (DIC) method [6,7] on a model material stainless steel 316L, and found experimental evidence of strain ratchetting in support of the hypothesis. A “critical” strain was also identified from the instantaneous strains at the locations near the crack tip as the crack approached. Encouraged by these results, we would like to further the research by mapping near tip strains in a HAZ of welds, and to examine if a “graded” microstructure and variation in its mechanical properties may affect the strain evolution and fatigue crack growth behaviour in this complex material environment. Due to the site-dependent material characteristics in a HAZ [1,2], full-field measurements were carried out *in situ* on welded specimens with a precrack in the HAZ. Specifically, the surface total strains in the region of interest were measured using Digital Image Correlation (DIC) and the bulk elastic strains in the volume of interest were mapped using Energy Dispersive X-Ray Diffraction (EDXD), both during the fatigue crack propagation experiments.

The basic principles of DIC, as a non-contact optical method for full-field displacement measurement, were established in the 1980’s [8], with algorithms [9] developed for more robust and faster convergence for a range of engineering applications. Sutton and his associates [9] were the first to use DIC in the studies of fatigue and fracture mechanics, when crack opening displacements were obtained post fatigue testing and image acquisition. Crack growth resistance was studied in a functionally graded material [10], where a region of K-dominance was identified. Fracture mechanics parameters, such as K, T and J, were identified from DIC analyses [11-14]. Fatigue crack growth has been studied using DIC by mapping near-tip strains [6, 7, 15, 16] or the plastic zones [17] during crack growth, some at sub-grain level [14,15] and *in situ* [6,7,17]. A limitation of DIC is that it can only track surface deformation, whilst bulk deformation is more relevant to structural integrity assessments. The latter may be examined using neutron diffraction or high energy X-ray diffraction, which measures the average elastic strains of a volume due to atomic lattice deformation [18]. For example, strain mapping by synchrotron X-Ray diffraction has been carried out in several studies of

fatigue crack growth, notably in the evaluation of fatigue crack closure in the presence of overloads [19, 20].

In this work, we have utilised i) DIC, and ii) DIC and EDXD simultaneously to measure, *in situ*, the normal strains in the field of a growing fatigue crack in welded steel specimens. Surface measurements were carried out in the Experiment i) first, to test the DIC method in capturing data *in situ* during a fatigue test and to obtain some baseline strain maps; whilst strains on the surface and in the bulk of the specimen were measured simultaneously in the Experiment ii) to obtain the full-field information. Prior to strain mapping, measurement uncertainties were evaluated under the relevant loading conditions to assess the influence of some key data processing parameters. The results from the surface and the bulk measurements are discussed, together with the role of key data processing parameters in the determination of a characteristic or “critical” strain for fatigue crack growth in a HAZ of welded specimens.

## **2. Material and Methods**

### *2.1 Material and specimens*

A welded Cr2Ni4MoV steel was used in the experiments. The chemical composition and the mechanical properties of the material are summarised in Table 1, with further detail given elsewhere [1]. Standard compact tension (CT) specimens were used for both i) & ii) Experiments, with a specimen thickness of 12.5 mm used for Experiment i) and a reduced specimen thickness of 6.5 mm used for Experiment ii) to facilitate effective X-ray penetration in the EDXD study. The specimens were obtained from a weld joint to include BM, WM and HAZ, as shown in Fig. 1. A heat treatment was carried out at 550 °C for 40h after welding to relax the residual stresses due to welding/machining. The HAZ consists of martensite and bainites, with a “graded” microstructure of former austenite grain sizes in a range from 7 to 30  $\mu\text{m}$  [1, 2] and finer grains away from the weld line (Fig. 2). Large grains up to 100  $\mu\text{m}$  in size are found in the region near the weld line as a result of more intense heat exposure. The WM consists predominantly of bainites with an average packet size

of about 100  $\mu\text{m}$ . A notch was produced by electro-discharge machining within the HAZ near the weld line to promote crack initiation in this region.

## 2.2 Mechanical testing

The specimens were pre-cracked using a load-shedding scheme with  $\Delta K = 13 \text{ MPa}\sqrt{\text{m}}$  ( $R = 0.1$ ),  $a/W = 0.3$  for Experiment i) and  $a/W = 0.35$  for Experiment ii) at the end of pre-cracking. All pre-cracks were initiated at the notch tip and subsequent crack propagations under fatigue loading were within the HAZ, although somewhat away from the weld line at a small angle between  $7^\circ$  and  $12^\circ$  from the global X-axis (Fig. 2). The strain results were obtained in the global coordinate system, where “normal strain” refers to the strain component Y perpendicular to the global X-axis. The crack tips were found to be located in the clusters small grains with an average grain size of approximately 7  $\mu\text{m}$ . The specimens were polished with 0.5  $\mu\text{m}$  silica and etched for about 30 seconds using a 3% nitric acid-ethanol solution in a region of interest of 10 mm by 10 mm around the crack tip. This exposed the microstructure of the region and provided sufficient surface contrast for DIC analysis of optical images (Fig. 2).

In the Experiment i), two tests were carried out using a 100 kN Instron servo-hydraulic testing machine at the University of Portsmouth, under constant amplitude tension-tension cyclic loading at a frequency of 1 Hz and a load ratio of 0.1 using a triangular waveform. Stress intensity factor ranges  $\Delta K$  of 25 and 30  $\text{MPa}\sqrt{\text{m}}$  (ASTM E647–13a) were applied, respectively, to achieve steady-state fatigue crack growth. Reference images were taken at the minimum loads, whilst images at the peak loads were taken periodically *in situ* during the crack growth. A hold period of 20 seconds was applied at the peak and the reference loads to facilitate image acquisition during testing.

Experiments ii) were carried out on a similar Instron servo-hydraulic testing machine (100 kN) at the JEEP I12 beamline of the Diamond Light Source Synchrotron X-ray facility. The pre-cracked specimen was tested under a stress intensity factor range of  $\Delta K=30 \text{ MPa}\sqrt{\text{m}}$  at  $R = 0.1$ , and frequency of 1 Hz.

## 2.3 Digital Image Correlation (DIC)

DIC is an optical method that uses reference and deformed images in a digital form and performs image correlation analyses to extract full-field information of surface deformation [9]. The method analyses the surface pattern shifts in discretised “subset” elements of images. An image correlation algorithm tracks the movement of these subsets from successive images and find the maximum of correlation between subsets on two or more corresponding images through cross-correlation. The procedure is repeated for all subsets, and displacement maps and strains are obtained for the whole image. For Experiment i), data capture and analysis were accomplished using a LaVision DIC system (LaVision GmbH, Göttingen, Germany), equipped with a 12 bit CCD camera attached to an optical microscope with a Schneider Kreuznach 50 mm lens and a 100 mm extension tube. Two LED flash lights were used to ensure appropriate lighting conditions. A specimen surface area of approximately  $1300\text{ }\mu\text{m} \times 1100\text{ }\mu\text{m}$  was imaged with  $2456 \times 2058$  pixels, resulting in a spatial resolution of  $0.54\text{ }\mu\text{m/pixel}$ . The displacement and strain analyses were thereafter carried out using the software DaVis (LaVision, version 8.4). A parametric analysis [21] was carried out to evaluate the influence of data processing parameters on the measurement uncertainties in the presence of high strain gradients and inhomogeneous deformation near a crack tip. Similar measurement strategies were used in Experiment i) and Experiment ii) where appropriate; and the total strains, including both elastic and plastic components, were obtained and reported for the DIC analyses in both experiments.

#### *2.4 Energy Dispersive X-Ray Diffraction (EDXD)*

Energy dispersive X-ray diffraction (EDXD) is a synchrotron X-ray characterisation technique that uses a multi-wavelength "white beam". A multi-element detector, at a fixed Bragg diffraction angle, records the full diffraction spectrum simultaneously from crystalline grains in the specimen that are suitably oriented for diffraction within a gauge volume that is defined by collimating slits. Relative shifts in the diffraction peak positions are used to measure the changes in crystal lattice parameters and hence the elastic strain. By rastering the sample through the beam, a 2D map of the elastic strains can be produced. The high energy and brilliance of synchrotron X-rays allows the technique to be used on thick metal samples with reasonable data collection times. EDXD was used to map the bulk elastic strains around a crack in the HAZ of welded specimen in Experiment ii). The specimen was

scanned by rastering in the global X (approximately along the crack plane) and Y (approximately perpendicular to the crack plane) directions, using a white X-ray beam collimated by slits to obtain a gauge volume of  $100\text{ }\mu\text{m} \times 100\text{ }\mu\text{m}$  over a length of approximately  $4500\text{ }\mu\text{m}$  in the Z (specimen thickness) direction. A region of interest of  $1.6\text{ mm} \times 1.3\text{ mm}$  on the X-Y plane around the projected crack path was examined at regular intervals during the crack growth. The diffracting gauge volume was centred in the mid-plane of the specimen thickness, and the mapped area contained 238 individual non-overlapping measurements. The elastic strains were calculated using the PyXe python script [22], and only the data from the (110) diffraction peak were presented for conciseness, as similar results were obtained for the (200) and the (211) peaks. Further details of the general experimental setup on the beamline may be found elsewhere [18]. Strain maps were acquired at the minimum load and at the maximum loads at cycles  $N = 100, 300, 400, 500, 750, 1000, 1250, 1500, 1750$  and  $2000$ .

During the EDXD measurements, DIC images were also acquired simultaneously to complement the bulk measurements. This was made possible by installing the EDXD detector and the DIC microscope next to each other, while the loading rig was mounted on a translation stage, so the specimen within the loading rig could be positioned alternately in the X-ray beam for EDXD measurements and in the view of the microscope for optical DIC imaging. Suitable X-ray protection (lead blankets) was provided for the DIC equipment when the X-ray beam was on. The translation stage positioning was carried out using a calibrated digital encoder, with a precision greater than  $\pm 10\text{ }\mu\text{m}$ .

### **3 Results**

#### *3.1 Measurement uncertainty & parameter evaluation using DIC*

Only strains in global Y-direction ( $\epsilon_{yy}$ ) are reported in this study, as they are close to the maximum principal strains that are considered to be most relevant to crack growth [4]. Although the cracks grew at a slight angle from the global X-axis (Fig. 2), the data have not been transformed onto a local coordinate system centred at the crack tip, since an increased level of noise was encountered at such an attempt. The purpose of the analysis is to evaluate the measurement uncertainty of the strains ahead

of a crack tip, where a large strain gradient coupled with microstructure variation in the HAZ presents a challenge to crack tip characterisation. The influence of the subset size and the size of the measurement window (MW) on the DIC measurements is considered of particular relevance to a robust and reproducible characterisation of the strains ahead of a crack tip, and this is summarised here following a parametric study [21]. The subset size is known to affect the noise level in DIC measurements [23-25]; whilst the measurement values are very sensitive to the size of the MW, an area used to obtain average displacement/strain values from all the data points inside of the MW. The standard deviation (STDV) is used to quantify random noise, which is a major source of errors in DIC measurements, as it can reach levels which overshadow the target deformation as well as the systematic (bias) errors. Besides, given that the true strain values near a crack tip are unknown, it is not possible to assess the bias errors; hence the selection of parameters has been mainly aimed at achieving low random errors indicated by STDV.

A typical displacement map, obtained from the Experiment i), is shown in Fig. 3(a), with the crack tip indicated. The crack tip position was initially determined by optical microscopy, and later verified from the DIC images. For the parametric analysis, four measurement points were selected (Fig. 3(b)) at an interval of  $3.4\ \mu\text{m}$ , which is about half of the average grain size in the HAZ region. Fig 3(c) illustrates the positions and the geometries of the measurement windows (MWs) for measurement point 1, which is the centre of the smallest MW. The larger MWs share the same left edge as the smallest MW. The same configuration applies to the other measurement points. Three specimens were studied for the exercise, with five images taken at each condition ( $n=15$ ).

Figure 4 shows the effects of subset size on the STDV of peak (a) normal displacement and (b) normal strain when the MW is fixed at  $37\times 37\ \text{pixels}^2$  for measurement position 1 (Figure 3 (b)) under the three selected loading conditions ( $K = 0, 20$  and  $30\ \text{MPa}\sqrt{\text{m}}$ ). The STDVs of both displacements and strains increase significantly with the decrease of subset size, particularly below  $49\times 49\ \text{pixels}^2$ , possibly due to insufficient information inside of small subsets that can be used for correlation. Under loads, the STDVs of displacement appear to increase slightly at larger subset size, although the



STDVs of strains appear to be consistently small ( $<0.2\%$ ) and insensitive to the applied load level for subset sizes of  $49 \times 49$  pixels<sup>2</sup> or larger.

The effects of the size of MW on the STDV of the mean values of displacement and strain of the MWs are assessed for 3 specimens with 5 images each ( $n=15$ ), and the results are shown in Figure 4(c, d), with a subset size fixed at  $49 \times 49$  pixels<sup>2</sup>. Once again, the STDVs are much higher in the loaded cases than those unloaded for both displacement and strain. With a greater number of displacement vectors for larger sizes of MW, the noise level seems to increase proportionally (Fig 4(c)); a similar trend is observed for the STDV of strains (Fig. 4(d)), although the effect of size of MW on the noise level seems to be less pronounced at larger sizes of MW (above 50 pixels for the unloaded and 130 pixels for the loaded cases).

The impact of subset size and the size of MW on the measured strains in the near-tip region (four positions labelled in Fig. 3(b)) is shown in Fig. 5. The results were obtained using the DIC analysis of the images captured at the selected K values. Clearly the measured strain values at a given position vary significantly with both the size of MW and subset size, particularly at small sizes of MW and subset. To perform an analysis near a crack tip where high displacement and strain gradients prevail, a compromise needs to be made between the spatial resolution, i.e. identifying the discrete values at the tracked positions, and obtaining strain values that are not significantly affected by the correlation or measurement parameters. For operational purposes, a size of MW was chosen to be  $37 \times 37$  pixel<sup>2</sup> and the subset size was chosen to be  $49 \times 49$  pixels<sup>2</sup> for the Experiment i). Using these parameters, the standard deviation of the measured strains under loads ( $20 < K \leq 30 \text{ MPa}\sqrt{\text{m}}$ ) is about 0.44 %.

### *3.2 In situ DIC measurements of strains during fatigue crack growth*

For Experiment i), a specimen was cyclically loaded at  $\Delta K = 25 \text{ MPa}\sqrt{\text{m}}$  ( $R = 0.1$ ) for 7000 cycles to achieve steady-state fatigue crack growth of  $960 \mu\text{m}$  in the HAZ, at a slight angle ( $7^\circ$ ) to the X-axis (Fig. 6a). The average crack growth rate was  $1.4 \times 10^{-7} \text{ m/cycle}$ . A second specimen was tested under  $\Delta K = 30 \text{ MPa}\sqrt{\text{m}}$  ( $R = 0.1$ ) for 4400 cycles, crack growth of  $1060 \mu\text{m}$  was obtained within the HAZ at an angle of  $12^\circ$  (Fig. 6b), with an average crack growth rate of  $2.4 \times 10^{-7} \text{ m/cycle}$ . The normal strains

( $\epsilon_{yy}$ ) were tracked at the selected observation points (Fig 6) along the crack paths *in situ* throughout the experiments. At each tracking position, the average strains were measured at a regular interval (every 200 cycles at  $\Delta K=25 \text{ MPa}\sqrt{\text{m}}$ ; every 100 cycles at  $\Delta K=30 \text{ MPa}\sqrt{\text{m}}$ ) until the crack tip passed this position. The positions were traced optically on the DIC images and matched with the positions on the strain maps.

The normal strains are found to increase rapidly with cycles as the crack tip approaches an observation point for both load cases (Fig.7). A “critical” strain ( $\epsilon_{cr}$ ) may be estimated from the average “onset” strains captured at all observation points when the crack tip reached them, with an average value of  $\epsilon_{cr} = 5.4\%$  (STDV = 0.7%) at  $\Delta K = 25 \text{ MPa}\sqrt{\text{m}}$  (Fig. 7(a)); and  $\epsilon_{cr} = 6.3\%$  (STDV = 0.9%) for  $\Delta K = 30 \text{ MPa}\sqrt{\text{m}}$  (Fig. 7(b)). Caution should be exercised with regard to these values though, as they depend on the sizes of subset and MW (Fig. 5), and emphasis is placed on their relative magnitudes under the same observation and analysis conditions. The current values were obtained using a subset size of  $49 \times 49 \text{ pixels}^2$ , with an overlap of approximately 90% due to a step size of 6 pixels, and a MW of  $37 \times 37 \text{ pixel}^2$  ( $20 \times 20 \mu\text{m}^2$ , 36 data points within the MW).

### 3.3 *In situ Measurement by EDXD and by DIC*

For Experiment ii), both surface and bulk strains were monitored during the experiment at Diamond. The bulk average elastic normal strains ( $\overline{\epsilon_{yy}^e}$ ) were obtained using the EDXD technique under tensile cyclic load corresponding to  $\Delta K = 30 \text{ MPa}\sqrt{\text{m}}$  and  $R = 0.1$ . A crack growth of approximately  $300 \mu\text{m}$  was produced over 2000 cycles. The crack growth was at a small angle about 5 degrees to the X-axis, with an average crack growth rate of  $1.7 \times 10^{-7} \text{ m/cycle}$  (see Appendix for details of the crack growth rate measurement). Simultaneously, the surface total strains ( $\epsilon_{yy}$ ) were also tracked using DIC. The size of MW used for the DIC analysis was chosen to be comparable to the gauge volume used in the EDXD, with a subset size of  $99 \times 99 \text{ pixels}^2$ ; an overlap of around 90% due to a step size of 9 pixels and the size of MW of  $185 \times 185 \text{ pixels}^2$  ( $100 \times 100 \mu\text{m}^2$ , 960 data points in MW). An error assessment for the EDXD analysis was performed using the data from ten successive scans at a single measurement point away from the crack tip, and the STDV was estimated to be 0.017.

Normal strains at eight selected points ahead of the pre-crack were tracked every 100 cycles along the perceived crack plane (Fig. 8) at the maximum loads. The distance between the strain measurement points was 100  $\mu\text{m}$  (0% overlap), with strain values representing the averages over the nominal gauge volume of 100  $\mu\text{m} \times 100 \mu\text{m} \times 4.5 \text{ mm}$  (neglecting beam spread). Fig. 9 shows the maximum strain evolution with cycles at the selected tracking points from both EDXD and DIC. A progressive increase in both normal elastic strain (bulk) and total strain (surface) is observed, as the crack tip approaches a given tracking point, similar to that observed on the surface by DIC previously (Fig. 7).

Accurate determination of the crack tip position during the crack growth is important, as errors in identifying its position may compromise the “onset” strain values obtained, affecting subsequently the estimation of the critical strain. The surface crack tip position was estimated from the optical DIC images within an error range about 18 pixels (10  $\mu\text{m}$ ), corresponding to two data points on the according displacement and strain map grid of 6 to 9 pixels (3 to 5  $\mu\text{m}$ ). The crack tip position was also determined by the peak strains from EDXD, following a comparison of optical DIC images with the EDXD data analysed by a cross-correlation method to achieve sub-pixel precision. The strain peaks identified by mapping of the bulk data are found to correlate closely with the crack tip positions obtained from the surface measurements. Full details are given in the Appendix to this paper.

Critical strains are estimated by averaging the strain values obtained at the selected observation points by EDXD and DIC when the crack tip reached these observation points, and the results are shown in Fig. 9. An average critical elastic strain of 0.63% ( $\pm 0.2$ ) was estimated in the bulk by EDXD; whilst surface measurements by DIC return a critical total strain of 1.54% ( $\pm 0.13$ ). These values were obtained using the same size of measurement window, i.e. 185 x 185 pixel<sup>2</sup> (100 x 100  $\mu\text{m}^2$ ) for both DIC and EDXD measurements, although the bulk strains are volume averages over a thickness of 4.5mm.

#### **4 Discussion**

Near-tip strain fields have been mapped *in situ* during fatigue crack growth for the first time within a HAZ of weld specimens, both in the bulk and on the surface of the specimens. Strain accumulation

has been observed in the bulk and on the surface as the crack approaches the selected measurement points, which is consistent in trend with that observed from the previous DIC measurements [6,7] and the numerical simulations of strain ratchetting [4,5]. Such information may be useful in the assessments of structural integrity of welded components, where fatigue crack growth in HAZ has been identified as a main failure mechanism [2]. Conventionally, only nominal crack growth rates of materials are obtained and taken in the life assessment procedures. The knowledge of full-field strain evolution with regard to fatigue crack growth in a HAZ will be useful in developing a micro-mechanics approach to fatigue crack characterisation in this complex region of interest, where a graded microstructure and variable material properties prevail. Significantly higher strength was found in the HAZ close to the weld line, and the strength decreases with distance from the weld line [1]. Our results show that the preferred path of fatigue cracks in the HAZ appears to be in a fine-grained region and at a slight angle from the perceived crack plane. The direction of crack growth seems to be towards a fine-grained zone with lower strength, consistent with the material characterisation [1, 26]. This information may be useful in exploring welding processes for favourable microstructures in promoting improved fatigue crack resistance.

Measurement of strains using the DIC method has become increasingly popular as a result of advances in computing technology and general availability of DIC facilities. However, measurement uncertainties are not always assessed for relevant applications. This oversight can have a significant negative impact on the measurement quality and fidelity, particularly in cases of large heterogeneous deformation. In this work, we have examined the impact of some of the key parameters on the measurement uncertainty and quantity near a crack tip, which is a region of large inhomogeneous deformation with high strain gradients. As shown in Fig. 4, loading appears to significantly influence the level of the measurement noise, particularly for small subset sizes and large sizes of MW. A subset size of about  $50 \times 50$  pixels<sup>2</sup> appears to yield lowest errors for both displacement and strain. On the other hand, the STDV of displacements appears to increase with the increase of the size of MW; whilst a similar trend is found for the STDV of strains, although to a somehow lesser degree. As strains are of the main interest in this work, the analysis parameters were chosen to offer low standard

deviations whilst maintaining sufficiently high spatial resolution (Fig. 5). Unlike finite element studies, where a convergence test would guide mesh configuration, DIC measurements rely on the surface markers, applied speckles or microstructure texture, which often dictate the choice of subset size and the size of MW. For small subset sizes, the measurement uncertainties tend to be high, whilst at large subset sizes the spatial resolution may be lost. As the true values of near tip strains are site-specific and largely unknown, the accuracy of the measurements cannot be assessed directly, although the results do show clearly the influence of the size of measurement window on the measured strain values (Fig. 5; Fig. 7 and Fig. 9).

The DIC parameters used in Experiment ii) necessarily differed from those used in Experiment i) in order to make a comparison with the data obtained from EDXD using a larger volume gauge size. The results from Experiment i) were reprocessed using the same as used in Experiment ii), and a critical strain (1.4%) was found to be very similar to that of Experiment ii) (1.5%, Fig 9). This further illustrates the influence of the size of MW on the measured strains, hence it is extremely important to note this limitation in experimental reporting. The chosen parameters are sufficiently representative of the experimental conditions to be used to examine the trends between observations, but the strain values reported must be interpreted together with the chosen correlation and measurement parameters. For this reason, the “critical” strain estimated from the average of measured “onset” strains when the crack tip reached the tracking points should not be taken as a unique material property.

Whilst the specimens used for surface and bulk measurements have different thicknesses due to the specific experimental requirements, the results from the surface DIC measurements in both cases should not be affected by the variation in specimen thickness, due to predominantly plane stress state on the specimen surfaces. The influence of specimen thickness on DIC measurements was investigated in [27] for specimens of thickness between 3 mm to 25 mm, and similar DIC results were obtained.

The elastic strains near a fatigue crack tip within the bulk of the material have been mapped in a HAZ for the first time. It is known that HAZ has a complex microstructure due to the welding process, and the material properties and microstructure in this particular type of weld are known to be varied [1]. In

the current study, however, steady-state crack growth was achieved; hence the influence of microstructure should be small. The bulk elastic strains measured by EDXD are lower than the surface total strains measured by DIC for the same size of MW, although these two quantities are not directly comparable for several reasons. First, EDXD measures elastic strain, whilst DIC measures the total strain. Secondly, the DIC measurements were obtained on the surface, where the lack of constraint leads to significant plastic deformation. The measured total strain may therefore contain a significant plastic component. EDXD, on the other hand, measured elastic strains averaged over a gauge volume of  $100\text{ }\mu\text{m} \times 100\text{ }\mu\text{m} \times 4.5\text{ mm}$ , under the assumption of a straight crack front. The crack front may not be perfectly straight, hence the measurements represent an approximate description of the average elastic strain field of the crack front.

A monotonic yield strain of  $\epsilon_{cr} \approx 0.5\%$  was reported for the material in the HAZ in a similar CrNiMoV rotor steel [26] measured in thin specimens (0.5mm). Although the critical bulk strain of  $\epsilon_{cr} \approx 0.6\%$  obtained by EDXD is similar to the yield strain, the latter is subject to measurement processing parameters hence the two values are not directly comparable.

There are some limitations to this study. Firstly, surface micro-texture produced by etching was used as features for the DIC analysis. Although this approach removes the ambiguity of painting speckles, it does rely on the uniform “randomness” of the micro-texture distribution, which is not guaranteed in the HAZ of the specimens as received. If a cluster of features happens to be away from the areas of interest, whilst features are sparsely distributed inside the areas of interest, this may adversely affect the measurement quality.

Furthermore, although bulk measurements were obtained by EDXD, the strains were averaged over a relatively large gauge volume with some uncertainty in the position and the shape of the crack front. The spatial resolution that can be achieved by EDXD is therefore lower than that of DIC. As only the elastic strains were measured in the bulk whilst total strains were measured in the surface, it is not possible to make a direct comparison between the two measurements, particularly when the influence of plasticity is more significant on the specimen surface than that in the bulk of the specimen.

## Conclusions

Fatigue crack growth behaviour in the heat-affected zone of a welded CrNiMoV steel has been examined *in situ* using DIC and EDXD. Normal strains ahead of the crack tip were mapped in the bulk and on the surface of the specimens during the process of fatigue crack growth. The measurement uncertainties and the average values of the strains seem to be sensitive to the correlation/measurement parameters, including subset size and the size of measurement window. Nonetheless, a characteristic “critical” strain may be estimated, on the surface and in the bulk of the specimen, based on the instantaneous onset strains captured as the crack tip reached the selected observation points. The critical bulk elastic strain, measured by EDXD, was found to be comparable to the yield strain of the material.

## Acknowledgements

The EDXD observations were carried out at JEEP I12 beamline of the UK Diamond Light Source as experiment EE13579. The assistance of A. Cinar (Sheffield University) with the phase congruency method (see appendix) is gratefully acknowledged.

## References

- [1] M.L. Zhu, F.Z. Xuan, Correlation between microstructure, hardness and strength in HAZ of dissimilar welds of rotor steels. *Mater. Sci. Eng. A* 527 (2010) 4035–4042.
- [2] M.L. Zhu, D.Q. Wang, F.Z. Xuan, S.T. Tu, Observation and modeling of physically short fatigue crack closure in terms of in-situ SEM fatigue test. *Mater. Sci. Eng. A* 618 (2014) 86–95.
- [3] P.C. Paris, M.P. Gomez, W.E. Anderson, A rational analytic theory of fatigue, *Trend Eng.* 13 (1961) 9–14. doi:10.11648/j.ijmea.s.2015030201.11.
- [4] L.G. Zhao, J. Tong, J. Byrne, The evolution of the stress – strain fields near a fatigue crack tip and plasticity-induced crack closure revisited, *Fatigue Fract Engng Mater Struct.* 27 (2004) 19–29.

- [5] L.G. Zhao, J. Tong, A viscoplastic study of crack-tip deformation and crack growth in a nickel-based superalloy at elevated temperature, *J. Mech. Phys. Solids*. 56 (2008) 3363–3378. doi:10.1016/j.jmps.2008.09.006.
- [6] J. Tong, B. Lin, Y.W. Lu, K. Madi, Y.H. Tai, J.R. Yates, V. Doquet, Near-tip strain evolution under cyclic loading: In situ experimental observation and numerical modelling, *Int. J. Fatigue*. 71 (2015) 45–52. doi:10.1016/j.ijfatigue.2014.02.013.
- [7] Y.-W. Lu, C. Lupton, M.-L. Zhu, J. Tong, In Situ Experimental Study of Near-Tip Strain Evolution of Fatigue Cracks, *Exp. Mech*. 55 (2015) 1175–1185. doi:10.1007/s11340-015-0014-4.
- [8] W.H. Peters, W.F. Ranson, Digital imaging techniques in experimental stress analysis, *Opt. Eng.* 21 (1982) 427–431. doi:10.1117/12.7972925.
- [9] M.A. Sutton, J.J. Ortu, H. Schreier, Image correlation for shape, motion and deformation measurements: Basic concepts, theory and applications, 1st ed., Springer US, Boston, MA, 2009. doi:10.1007/978-0-387-78747-3.
- [10] J. Abanto-Bueno, J. Lambros, Investigation of crack growth in functionally graded materials using digital image correlation, *Eng. Fract. Mech.* 69 (2002) 1695–1711. doi:10.1016/S0013-7944(02)00058-9.
- [11] S. Roux, J. Réthoré, F. Hild, Digital image correlation and fracture: an advanced technique for estimating stress intensity factors of 2D and 3D cracks, *J. Phys. D: Appl. Phys.* 42 (2009) 214004. doi:10.1088/0022-3727/42/21/214004.
- [12] F. Mathieu, F. Hild, S. Roux, Identification of a crack propagation law by digital image correlation, *Int. J. Fatigue*. 36 (2012) 146–154. doi:10.1016/j.ijfatigue.2011.08.004.
- [13] P. Lopez-Crespo, B. Moreno, A. Lopez-Moreno, J. Zapatero, Characterisation of crack-tip fields in biaxial fatigue based on high-magnification image correlation and electro-spray technique, *Int. J. Fatigue*. 71 (2015) 17–25. doi:10.1016/j.ijfatigue.2014.02.016.



- [14] T.H. Becker, M. Mostafavi, R.B. Tait, T.J. Marrow, An approach to calculate the J-integral by digital image correlation displacement field measurement, *Fatigue Fract. Eng. Mater. Struct.* 35 (2012) 971–984. doi:10.1111/j.1460-2695.2012.01685.x.
- [15] J.D. Carroll, W. Abuzaid, J. Lambros, H. Sehitoglu, High resolution digital image correlation measurements of strain accumulation in fatigue crack growth, *Int. J. Fatigue*. 57 (2013) 140–150. doi:10.1016/j.ijfatigue.2012.06.010.
- [16] J.D. Carroll, W.Z. Abuzaid, J. Lambros, H. Sehitoglu, On the interactions between strain accumulation, microstructure, and fatigue crack behavior, *Int. J. Fract.* 180 (2013) 223–241. doi:10.1007/s10704-013-9813-8.
- [17] M. Besel, E. Breitbarth, Advanced analysis of crack tip plastic zone under cyclic loading, *Int. J. Fatigue*. 93 (2016) 92–108. doi:10.1016/j.ijfatigue.2016.08.013.
- [18] M. Drakopoulos, T. Connolley, C. Reinhard, R. Atwood, O. Magdysyuk, N. Vo, M. Hart, L. Connor, B. Humphreys, G. Howell, S. Davies, T. Hill, G. Wilkin, U. Pedersen, A. Foster, N. De Maio, M. Basham, F. Yuan, K. Wanelik, I12: The Joint Engineering, Environment and Processing (JEEP) beamline at Diamond Light Source, *J. Synchrotron Radiat.* 22 (2015) 828–838. doi:10.1107/S1600577515003513.
- [19] J.P. Belnoue, T.S. Jun, F. Hofmann, B. Abbey, A.M. Korsunsky, Evaluation of the overload effect on fatigue crack growth with the help of synchrotron XRD strain mapping, *Eng. Fract. Mech.* 77 (2010) 3216–3226. doi:10.1016/j.engfracmech.2010.08.018.
- [20] P. Lopez-Crespo, A. Steuwer, T. Buslaps, Y.H. Tai, A. Lopez-Moreno, J.R. Yates, P.J. Withers, Measuring overload effects during fatigue crack growth in bainitic steel by synchrotron X-ray diffraction, *Int. J. Fatigue*. 71 (2015) 11–16. doi:10.1016/j.ijfatigue.2014.03.015.
- [21] T. Wigger, C. Lupton, M. Zhu, J. Tong, A parametric study of DIC measurement errors of cracked dissimilar metals, *Strain*, under review.
- [22] C. Simpson, PyXe, (2016). doi:10.5281/zenodo.50185.

- [23] H. Schreier, M. Sutton, Systematic Errors in Digital Image Correlation Due to Undermatched Subset Shape Functions, *Exp. Mech.* 42 (2002) 303-310. doi:10.1177/001448502321548391
- [24] S. Yaofeng, J. Pang, Study of optimal subset size in digital image correlation of speckle pattern images, *Opt. Lasers Eng.* 45 (2007) 967-974. doi:10.1016/j.optlaseng.2007.01.012
- [25] B. Pan, H. Xie, Z. Wang, K. Qian, Z. Wang, Study on subset size selection in digital image correlation for speckle patterns, *Opt. Express.* 16 (2008) 7037-7048. doi:10.1364/OE.16.007037
- [26] M.L. Zhu, F.Z. Xuan, Effect of microstructure on strain hardening and strength distributions along a Cr-Ni-Mo-V steel welded joint, *Mater. Des.* 65 (2015) 707–715. doi:10.1016/j.matdes.2014.09.076.
- [27] P. De Matos and D. Nowell, Experimental and numerical investigation of thickness effects in plasticity-induced fatigue crack closure, *Int. J. Fatigue.* 31 (2009) 11-12. doi:10.1016/j.ijfatigue.2008.12.003

## **Appendix: Identifying the crack tip position of a growing crack by EDXD strain mapping**

### **Introduction**

Identifying the crack tip position from the elastic strain maps of EDXD is challenging due to the coarse spacing of the diffraction data ( $100\text{ }\mu\text{m} \times 100\text{ }\mu\text{m}$ ) and the localised strain field of the crack tip. A further complication arises due to the intermittent nature of the experiment where the sample stage was physically translated between diffraction scans to allow DIC images to be taken, and the fact that the crack propagated during the experiment. Consequently, each diffraction map and optical image was centred on a slightly different point.

A method has been developed based on an analysis of 2D maps of the diffraction peak width (FWHM), and inspired by DIC. Crack tip plasticity increases the diffraction peak width, so this provides a “characteristic” signal for the crack tip. The peak width was used in this analysis, but parameters such as peak intensity or elastic strain would yield similar results. In each map, the maximum FWHM occurs in the same pixel that measured the maximum elastic strain, forming a peak with lower values of FWHM in the surrounding pixels. Tracking the position of the FWHM peak using cross-correlation allows its movement to be measured with sub-pixel accuracy relative to its position in a reference map, and hence tracking the crack tip position. The method assumes that the spatial variation of the FWHM peak has the same functional form throughout the experiment.

### **Method**

To obtain maps of the diffraction peak width, Gaussian functions were fitted to the (110) diffraction data from each of the 23 energy dispersive detectors for each measurement point. The peak intensity as a function of the scattering vector is reported and treated here as a dimensionless parameter. The full-width at half-maximum (FWHM) was extracted for each diffraction peak from the fitting parameters, and the mean of the 23 FWHM values was used as the characteristic measurement at that point in the map. A typical map is shown in Figure A1a, in which a peak of FWHM is clearly visible, but its position cannot be determined by inspection to better than one pixel resolution, which is  $50\text{ }\mu\text{m}$  in this example.

The cross-correlation algorithm is based on the “Efficient subpixel image registration algorithms” of Guizar-Sicairos et al [A1], which takes a single-step discrete fourier transform of an upsampled image to register the images with a sub-pixel accuracy that is defined by the upsample factor. The first FWHM map in a sequence is defined as the ‘reference image’. Subsequent maps are known as the ‘images to register’. The reference and test images are fourier transformed using the MATLAB 2-dimensional fast fourier transform function *fft2*, and then passed to the cross-correlation function *dftregistration* [A2]. This registers the test image onto the reference image and outputs the image shift (in pixels) that would register the two images. The image shift is given to a precision equal to the inverse of the upsample factor – a 100x upsampling allows registration to within 0.01 pixels. The actual position of the sample stage was provided, from an encoder readout, to an accuracy of better than  $\pm 10 \mu\text{m}$ . These values provided the “stage shift”, and summing the image shift and the stage shift results provides the total movement of the peak position.

The analysis was applied to the data obtained during the first loading of the fatigue pre-crack over 1000 cycles at a stress intensity factor range ( $\Delta K$ ) of  $15.5 \text{ MPa}\sqrt{\text{m}}$  (load ratio  $R=0.1$ ). The optical observations show no crack propagation over this period. In this observation, the EDXD measurements were obtained with slits of  $100 \mu\text{m} \times 100 \mu\text{m}$ , with a 50% overlap, hence the pixel size of the data is  $50 \mu\text{m}$ . The correlation of the FWHM data, measured at  $K_{\text{max}}$ , found that the peak position changed overall by less than  $60 \mu\text{m}$  relative to the centre of the pixel that had the maximum FWHM at 0 cycles, with a movement in both X and Y directions that stabilised after a few hundred cycles (Figs A1b). The uncertainty in the change of peak position comprises a conservative  $\pm 10 \mu\text{m}$  uncertainty for the stage position encoder and the uncertainty due to the cross-correlation procedure. The latter is difficult to quantify, but can be done by assuming that the shape of the strain profile remains constant; in this case the correlation is theoretically accurate to within the precision of the registration ( $\sim 0.01$  pixels in this case, or  $0.5 \mu\text{m}$ ), so the encoder uncertainty is dominant. The measured peak position movement is larger than the maximum expected change in cyclic plastic zone size that could be caused by the increase in  $K_{\text{max}}$  relative to the pre-cracking condition. This would be expected to shift the centroid of the strained region. The change in plastic zone size for an increase in

K from  $\sim 13$  to  $\sim 16$  MPa $\sqrt{\text{m}}$  is estimated conservatively using the classical Rice approximation [A3] to be less than  $30\text{ }\mu\text{m}$  for a HAZ yield stress of 800 MPa (plane stress assumed). Consequently, the movement is judged to be largely due to localised deformation at the loading pins of the CT specimen, which cause a small movement of the specimen that stabilises within a few hundred cycles..

### **Analysis of the propagating fatigue crack**

The method was applied to the EDXD data obtained for the propagating fatigue crack, loaded at  $\Delta K = 30$  MPa $\sqrt{\text{m}}$  and  $R=0.1$  (described in the main text of this paper), and found that the FWHM peak position advanced  $315 \pm 10\text{ }\mu\text{m}$  in the X-direction and  $15 \pm 10\text{ }\mu\text{m}$  orthogonally; the change in X position was linear with the number of cycles with an average growth rate of  $0.167\text{ }\mu\text{m/cycle}$  (Fig A2).

The change in the surface position of the crack tip was also obtained by a DIC analysis of the optical images that were recorded during the Experiment ii). High precision measurements are challenging due to experimental difficulties in control of lighting and positioning of the camera, caused by the translations of the loaded specimen between the EDXD and optical observations. To address this, an image registration procedure was used to shift and crop the images to remove large displacements between successive images. The MATLAB code was based on the *dfregistration* function [A2] used in the analysis of the EDXD data. This produced a stack of similarly-sized images, which could be processed in the DaVis software; this was done using the legacy FFT (Fast Fourier Transform) DIC algorithm, with a final subset size of  $32 \times 32$  image pixels at 75% overlap.

Post-processing of the displacement field data was applied to determine the change in crack tip position on the specimen surface. The analysis implemented a phase congruency edge detection method, with a median filter applied to detect and remove outliers from the y-displacement field. It follows the approach developed by Cinar et al [A4], and has been found to be quite robust to noisy DIC data. First, the displacement component perpendicular to the global X-axis was extracted from the DIC data, and the MATLAB *inpaint\_nans.m* function [A5] was used to interpolate those data points that had no value (i.e. where the DIC cross-correlation algorithm failed to find a solution with

sufficient confidence). Outlier values were then identified and removed using a 2D median filter, with the *inpaint\_nans.m* function applied to re-interpolate the data, so creating a smoothed dataset. The displacement discontinuity along the crack could then be identified using the phase congruency function (*phasecongmono.m* [A6]), from which the crack tip position was measureable with a precision of 8 pixels (0.54  $\mu\text{m}/\text{pixel}$ ). This was estimated from the interval between displacement vectors obtained at a subset size of 32 x 32 pixels at 75% overlap.

The change in position of the EDXD FWHM peak and the measurements of the change in crack tip position by the phase congruency analysis of the DIC data are compared in Fig. A2. They are in good agreement and demonstrate that the EDXD data provide a good measure of the crack tip position. The EDXD data run slightly ahead of the surface measurements, typically by up to 50  $\mu\text{m}$ . The applied loading was adjusted as the crack extended to maintain a constant stress intensity factor range, so there should be no significant changes in the size of the crack tip plastic zone, therefore this difference might be due to the change in the curvature of the crack front within the specimen, the variation of the material properties within the HAZ, or the interaction of the fatigue crack with local microstructure that affect the surface propagation. As phase congruency detects the discontinuity of the crack opening, it is insensitive to crack tip plasticity, and has been shown to reliably find the crack tip [A4].

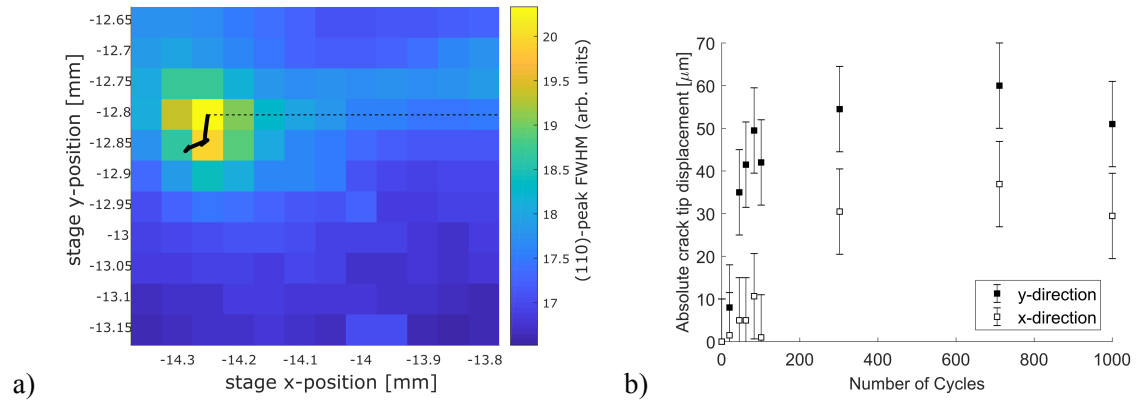


Figure A1: Measurement of the peak shift using maps of the (110) diffraction FWHM: a) The peak position, observed over 1000 cycles at  $\Delta K = 15.5 \text{ MPa}\sqrt{\text{m}}$  ( $R=0.1$ ), is measured relative to the background map obtained for the pre-crack when loaded to  $K_{\text{max}}$  at 0 cycles. The FWHM is shown in scaled dimensionless units and the pre-crack is indicated by a dotted line; b) numerical data for the measured relative change in the y-coordinate of the FWHM peak for the fatigue pre-crack, observed over 1000 cycles at  $\Delta K = 15.5 \text{ MPa}\sqrt{\text{m}}$ .

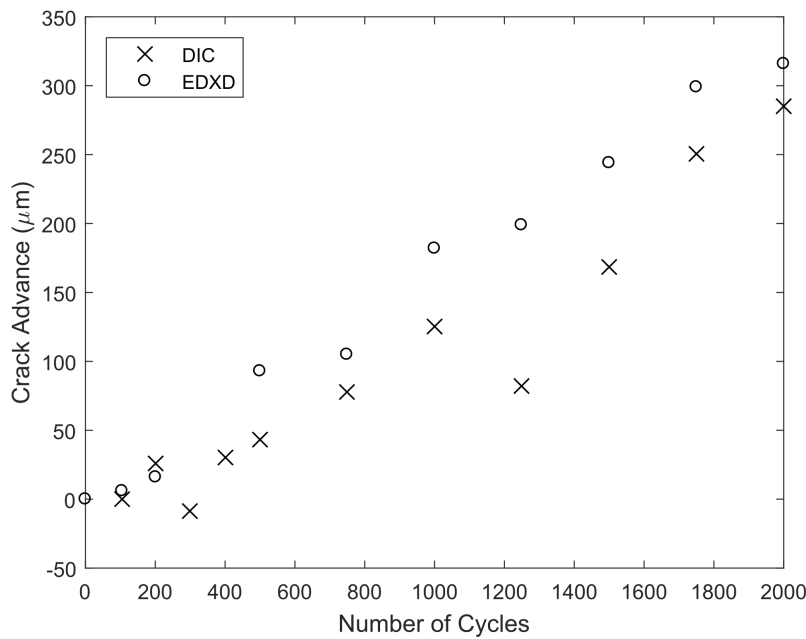


Fig A2: Comparison between the change in FWHM peak position, measured by cross-correlation of the EDXD maps, and the change in surface crack tip position measured by DIC analysis of optical images. The fatigue crack was propagated at  $\Delta K = 30 \text{ MPa}\sqrt{\text{m}}$  ( $R=0.1$ ) over 2000 cycles.

## References

- A1 Guizar-sicairos, M., Thurman, S. T. & Fienup, J. R. Efficient subpixel image registration algorithms. *Optical Letters* 33, 156–158 (2008).
- A2 Guizar, M. Efficient subpixel image registration by cross-correlation. (2016). at <https://uk.mathworks.com/matlabcentral/fileexchange/18401-efficient-subpixel-image-registration-by-cross-correlation>
- A3 Rice J.R. (1967) Mechanics of crack tip deformation and extension by fatigue, *Fatigue Crack Propagation*, ASTM STP 415, Am. Soc. Testing Mats, p.247
- A4. Cinar, A.F., Barhli, S.M., Hollis, D., Flansbjer, M., Tomlinson, R.A., Marrow, T.J., and Mostafavi, M. (2017) An autonomous surface discontinuity detection and quantification method by digital image correlation and phase congruency. *Optics and Lasers in Engineering*, 96, 94–106.
- A5 D’Errico, J. inpaint\_nans. (2012). at <http://uk.mathworks.com/matlabcentral/fileexchange/4551-inpaint-nans>
- A6 Kovesi, P. D. MATLAB and Octave Functions for Computer Vision and Image Processing. (2000). at <http://www.peterkovesi.com/matlabfns/>



| Chemical composition |             |         |           |          |           |         |            |             | Mechanical properties |                      |         |
|----------------------|-------------|---------|-----------|----------|-----------|---------|------------|-------------|-----------------------|----------------------|---------|
| Alloy (wt.%)         | C           | Cr      | Ni        | Mo       | V         | Mn      | Si         | Cu          | $\sigma_{YS}$ (MPa)   | $\sigma_{UTS}$ (MPa) | E (GPa) |
| BM, HAZ              | $\leq 0.35$ | 1.5-2.0 | 3.25-3.75 | 0.25-0.6 | 0.07-0.15 | 0.2-0.4 | $\leq 0.1$ | $\leq 0.15$ | 814.3                 | 910.6                | 217.7   |
| WM                   | 0.19        | 0.75    | 2.35      | 0.71     |           | 1.54    | 0.42       |             | 772.4                 | 833.9                | 210.4   |

Table 1. A summary of the chemical composition and the mechanical properties of the specimen [1].

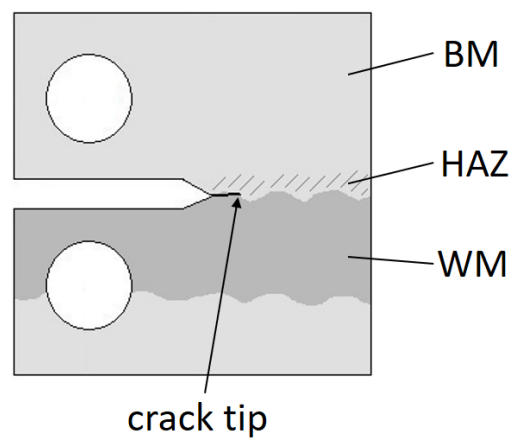


Figure 1. A schematic of the welded CT specimen, showing base metal (BM), weld metal (WM), heat affected zone (HAZ) near the weld line and a pre-crack in the HAZ.

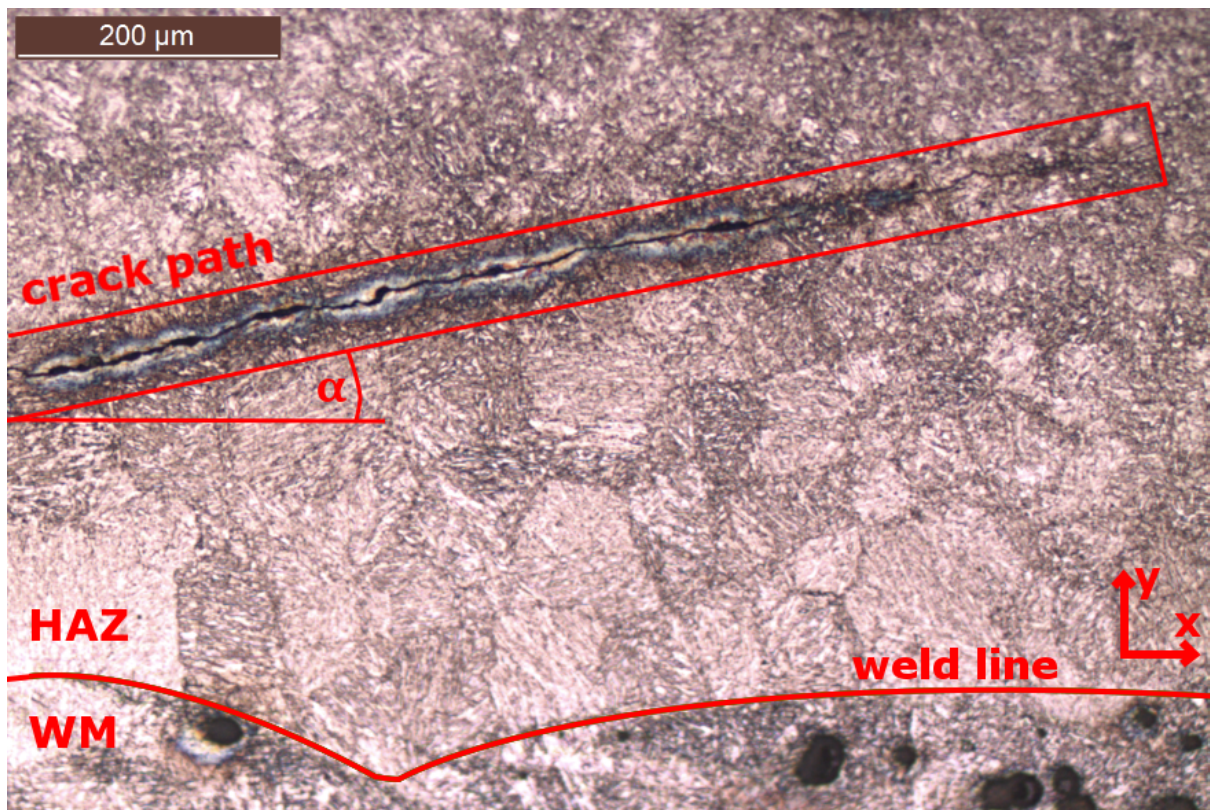


Figure 2. A typical pre-crack in the HAZ, with a slight angle  $\alpha$  from the X-axis. The grain sizes are around 100  $\mu\text{m}$  near the weld line and about 7  $\mu\text{m}$  near the crack tip. The specimen surface features exposed after etching were used for DIC image capture and correlation.

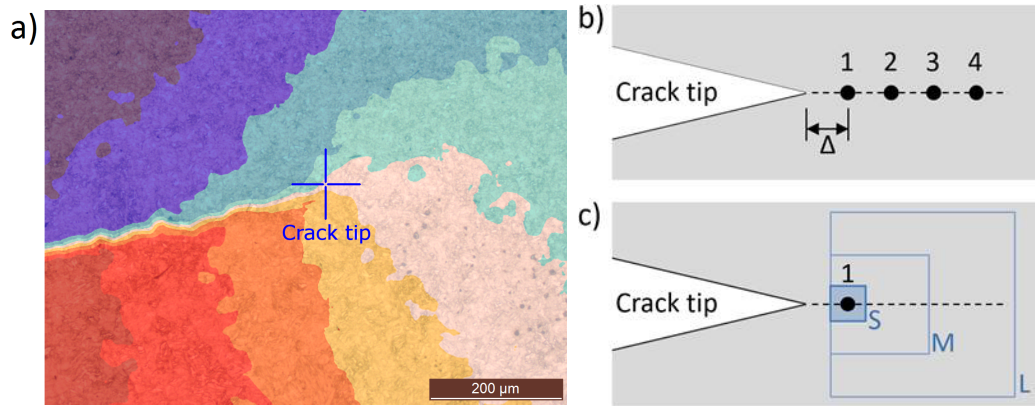


Figure 3. (a) A typical displacement map in y-direction with the crack tip marked (taken at  $\Delta K = 25 \text{ MPa}\sqrt{\text{m}}$ ,  $R = 0.1$ ), superimposed on a surface micrograph; (b) the selected measurement positions (1-4) ahead of the crack tip, where the distance between the points is  $\Delta$  ( $= 6$  pixels or  $3.25 \text{ }\mu\text{m}$ ) and (c) an illustration of the measurement windows (MWs) (S:  $12 \times 12 \text{ pixels}^2$ ; M:  $37 \times 37 \text{ pixels}^2$ ; L:  $56 \times 56 \text{ pixels}^2$ ) used for the parametric study at point 1 (b). The distance from the centre of the smallest MW to the crack tip is  $\Delta$ ; whilst all MWs share a common edge.

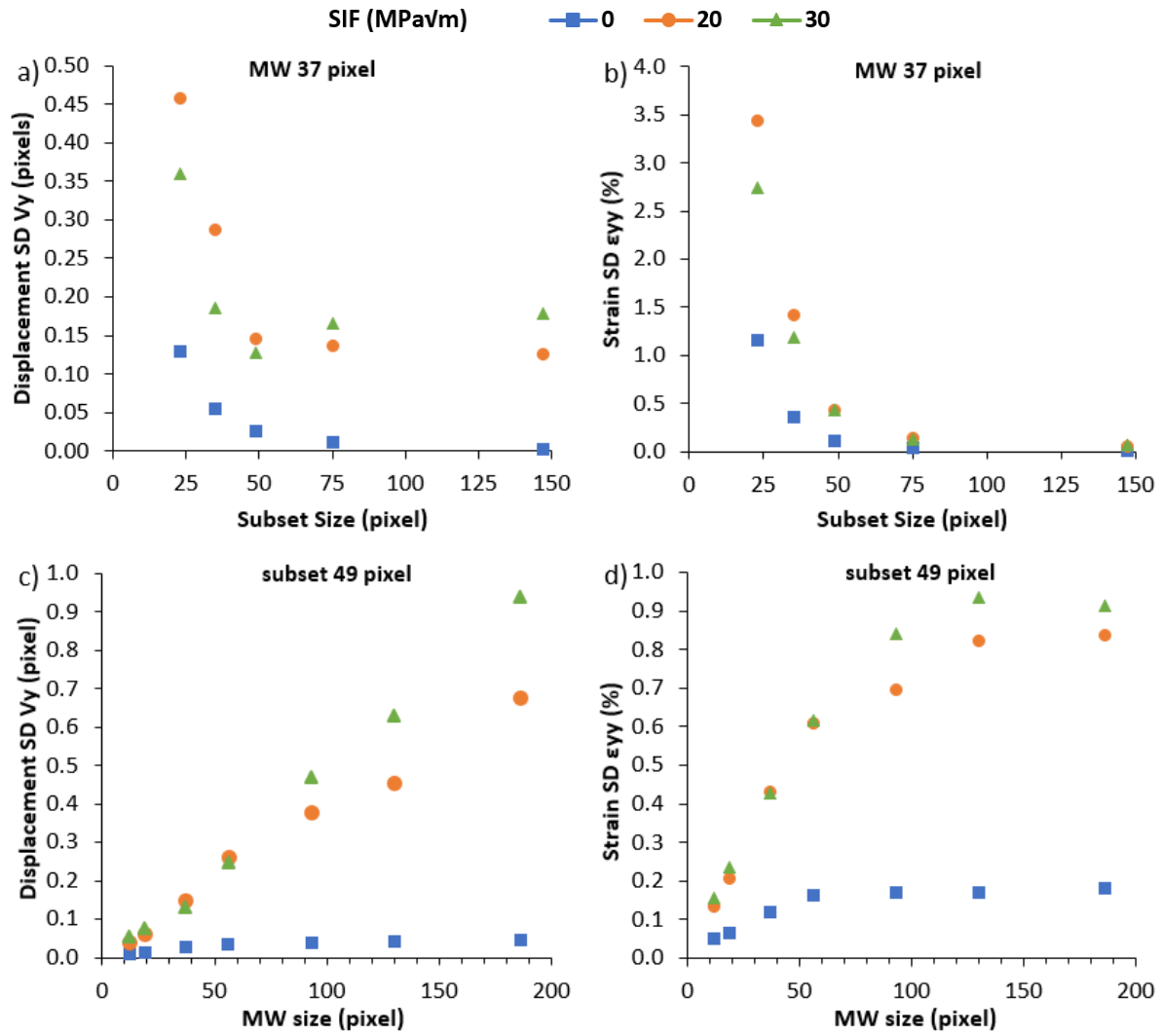


Figure 4. The effects of subset size on the STDV of (a) normal displacement and (b) normal strain (MW = 37 pixel); the effects of the size of measurement window (MW) on the STDV of (c) normal displacement and (d) normal strain (subset size = 49 pixel). The data are obtained ahead of the crack tip at the measurement position 1 (Figure 3 (b)) under three selected loading conditions (stress intensity factor (SIF) = 0, 20 and 30 MPa√m). The results are the mean values from 3 specimens with 5 images each (n=15).

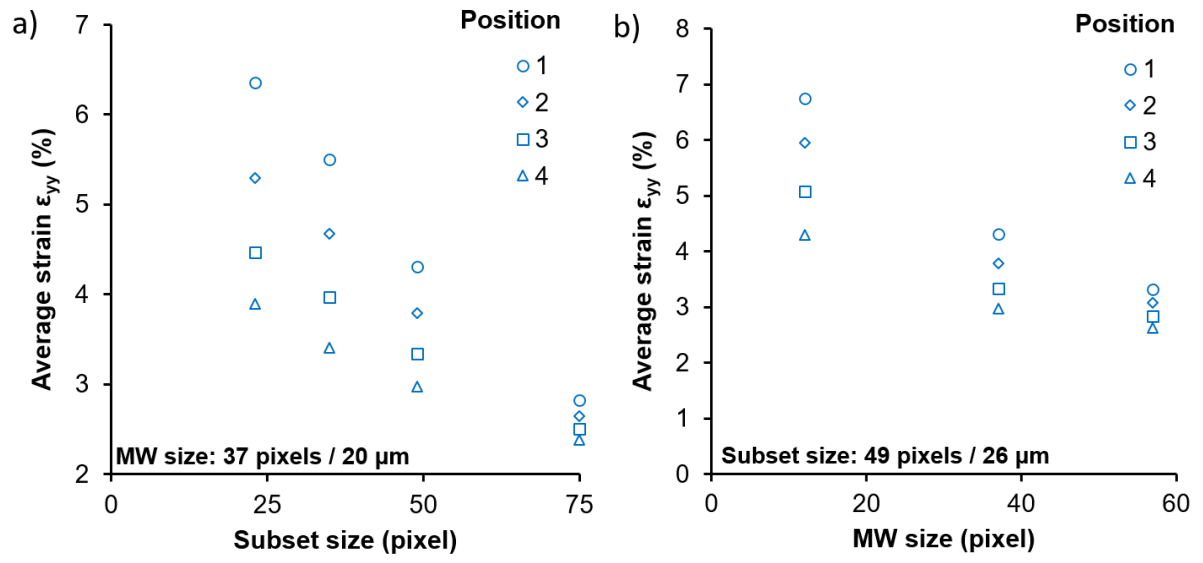


Figure 5. The effects of (a) subset size and (b) the size of MW on the measured average normal strains under  $K = 25 \text{ MPa}\sqrt{\text{m}}$  at the four measurement positions (Figure 3 (b)) ahead of the crack tip.

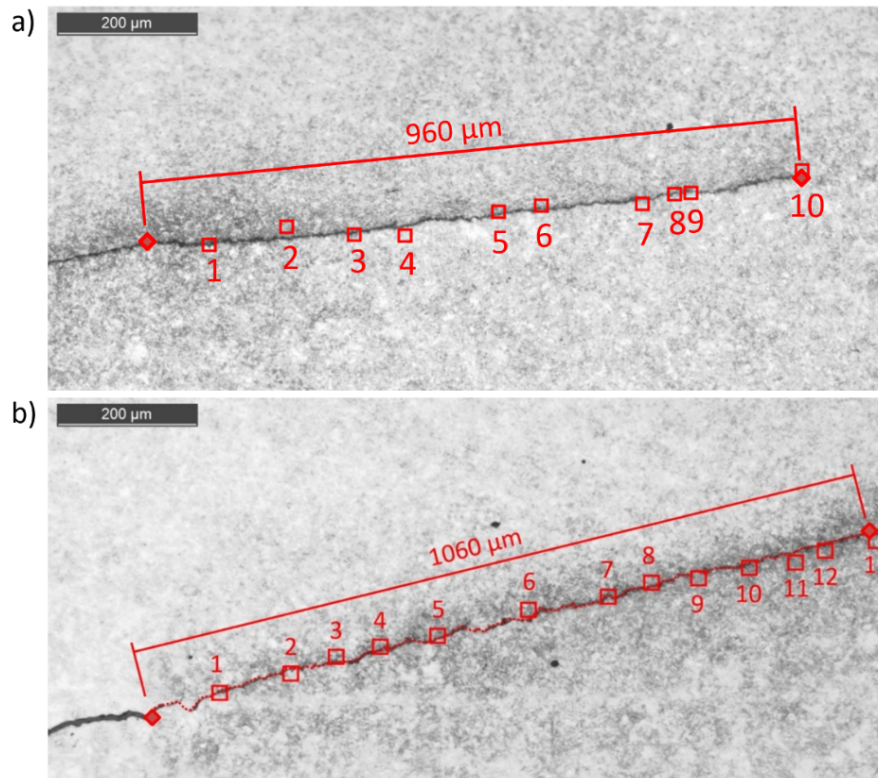


Figure 6. The fatigue crack profiles in the HAZ under (a)  $\Delta K = 25 \text{ MPa}\sqrt{\text{m}}$ ,  $R = 0.1$ ; (b)  $\Delta K = 30 \text{ MPa}\sqrt{\text{m}}$ ,  $R = 0.1$ . Normal strains were monitored ahead of the crack tip at the selected positions indicated.



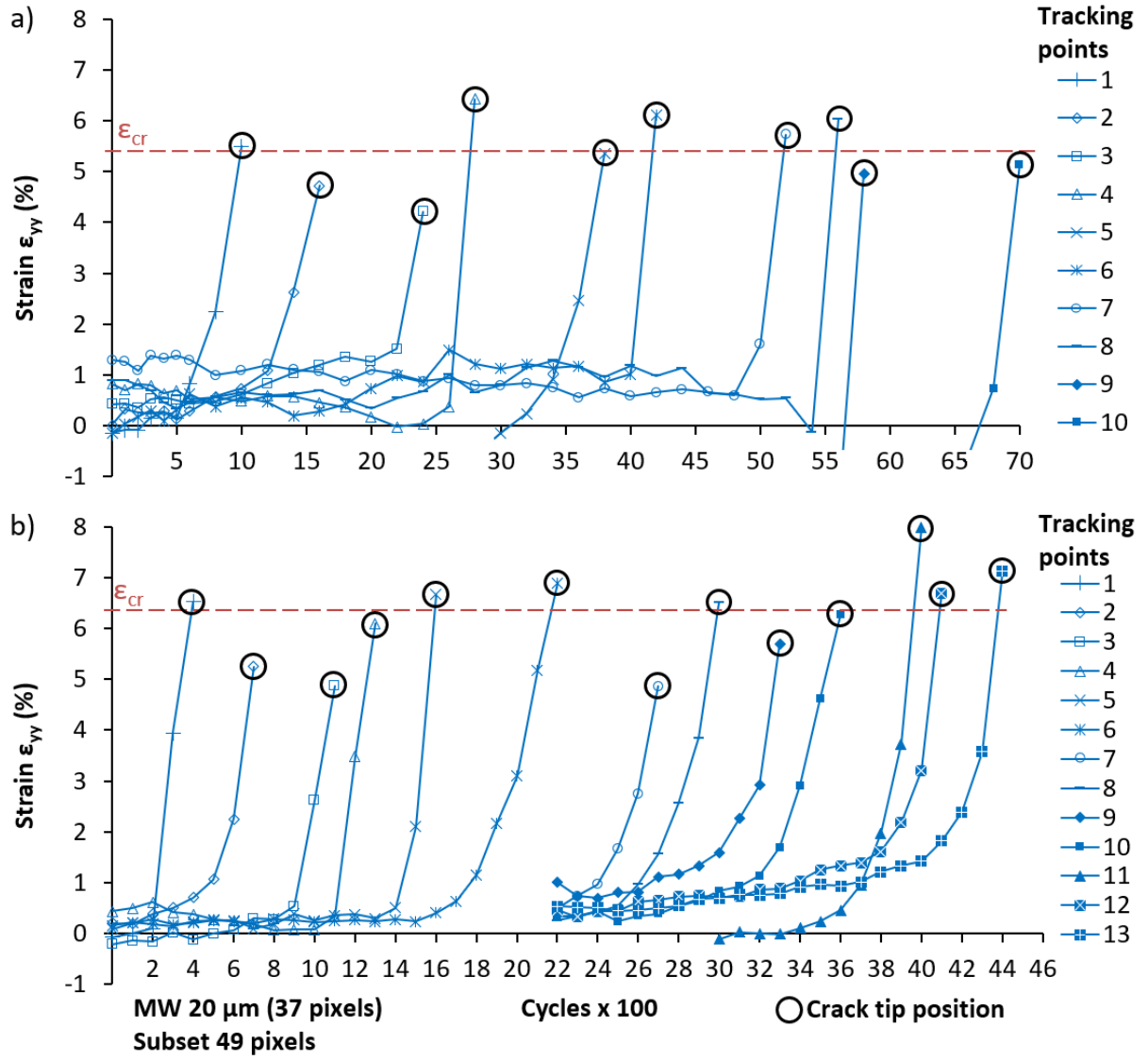


Figure 7. The normal strains recorded as a function of cycles, tracked at (a) the 10 positions on the crack path shown in Figure 6 (a) under a stress intensity of  $\Delta K$  25 MPa $\sqrt{\text{m}}$ ; and (b) the 13 positions shown in Figure 6 (b), using MW = 37 pixel (20  $\mu\text{m}$ ) under  $\Delta K$ =30 MPa $\sqrt{\text{m}}$ . The black circles indicate the onset strains when the crack tip reached the measurement positions.

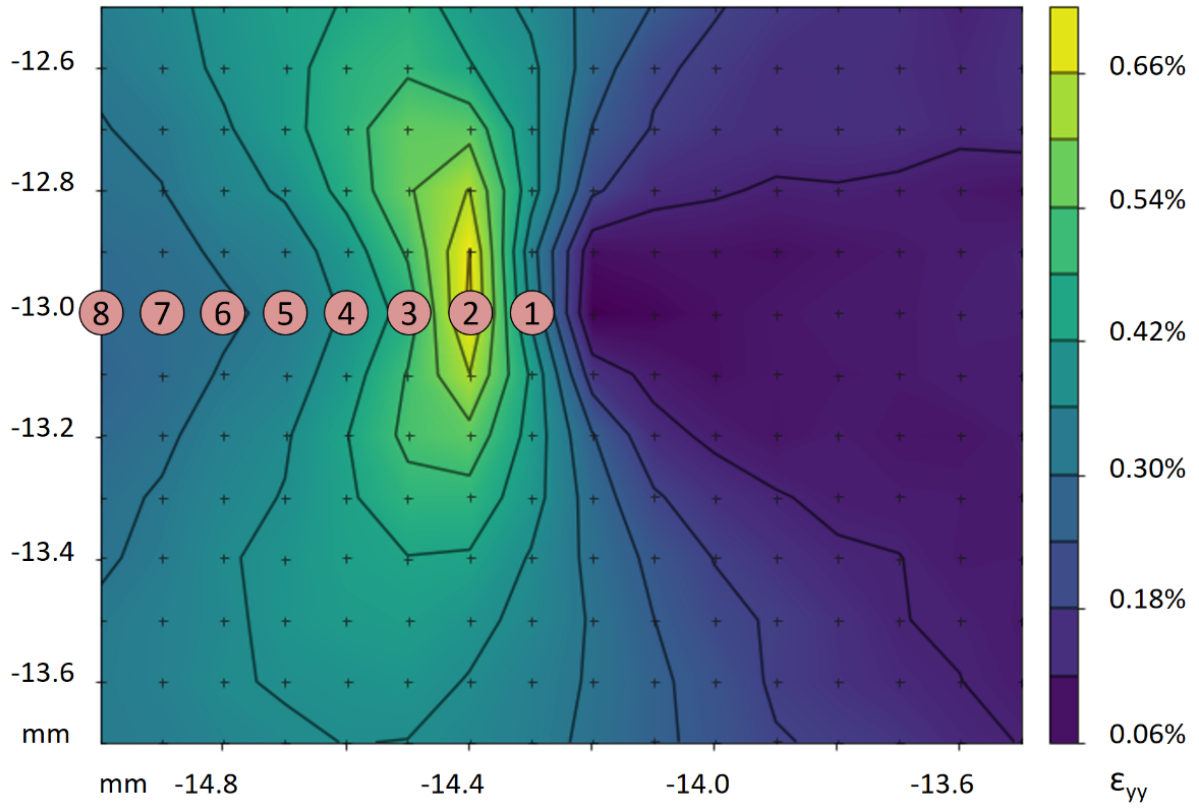


Figure 8. A typical strain map obtained from EDXD ( $K_{\max} = 33 \text{ MPa}\sqrt{\text{m}}$ ) and the selected tracking positions (1-8) along the crack path. The X and Y axes are the measurement coordinates of the sample positioning stage, and the individual measurement points are marked by the small crosses.



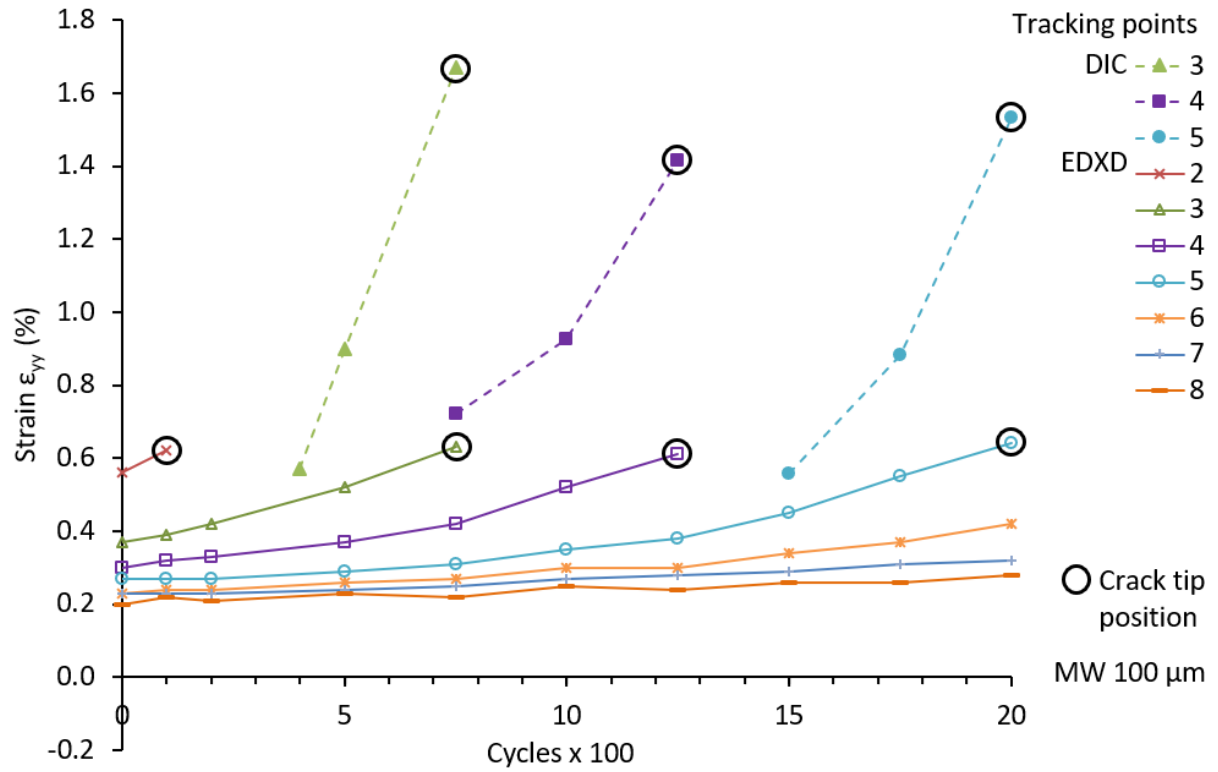


Figure 9. The evolution of the maximum normal strains captured by EDXD at the tracking points (Figure 8); and the surface normal strains obtained simultaneously by DIC. A “critical strain”  $\epsilon_{cr}$  may be estimated from the onset strains (black circles) when the crack tip reached the measurement points. The bulk critical strain is obtained as  $\epsilon_{cr} \approx 0.6\%$  (EDXD) and the surface critical strain as  $\epsilon_{cr} \approx 1.5\%$  (DIC).